

Structural, Morphological, and seismic evidence of Abbar region Active Tectonics in Western Alborz, NW Iran

Abstract

In this research, structures, geometries and directions of dominant stresses in the Abbar region (northwestern Iran) were examined. The fractures and lineaments of the area adequately matches to the brittle left-lateral shear zone model, and the two main fault systems of the area correlate with the P and R2 orders in the shear zones, respectively, where shear occurs along an approximate S60°E direction. Prior to the Quaternary, a compressive tectonic regime has governed the Abbar region along the NW-SE direction. Since the early Quaternary, this regime has changed to left-lateral shear along the WSW-ENE maximum stress direction. Thus, the reverse faults of the old regime have converted to strike-slip faults with reverse components. The geomorphological evidences such as fault scarps, Quaternary displacements and stream shifts indicate a high tectonic activity in the region. The major faults of the north of Abbar area can be divided into two groups with approximate directions of S50°E and N37°E. The Neotectonic activities of the region are in accordance with the left-lateral movement of the Manjil fault (as an important seismic fault in the western Alborz range) which has caused the formation of brittle structures and severe topographical changes.

Keywords: Abbar, Shear zone, Neotectonic, Western Alborz, Iran

1- Introduction

Natural disasters such as earthquakes cause negative impact on societies as well as divesting effects on infrastructures [1]. However, Neotectonic studies especially research on young tectonic phenomena and processes furnish developers with information which they need to address seismic hazards to prevent problematic issues in active tectonic regions [2]. In this research, some studies were conducted in Abbar region to specify tectonic regime of this area.

The study region is located in the NE of Zanzan province at the western Alborz structural zone, Iran (Fig.1a and 1b). The Alborz is a part of the Alpine-Himalayan orogeny belt in Western Asia. In the Abbar region, rocks of various ages from Paleozoic to Quaternary are exposed, and in some cases these rocks are separated from each other by faults (Fig.2).

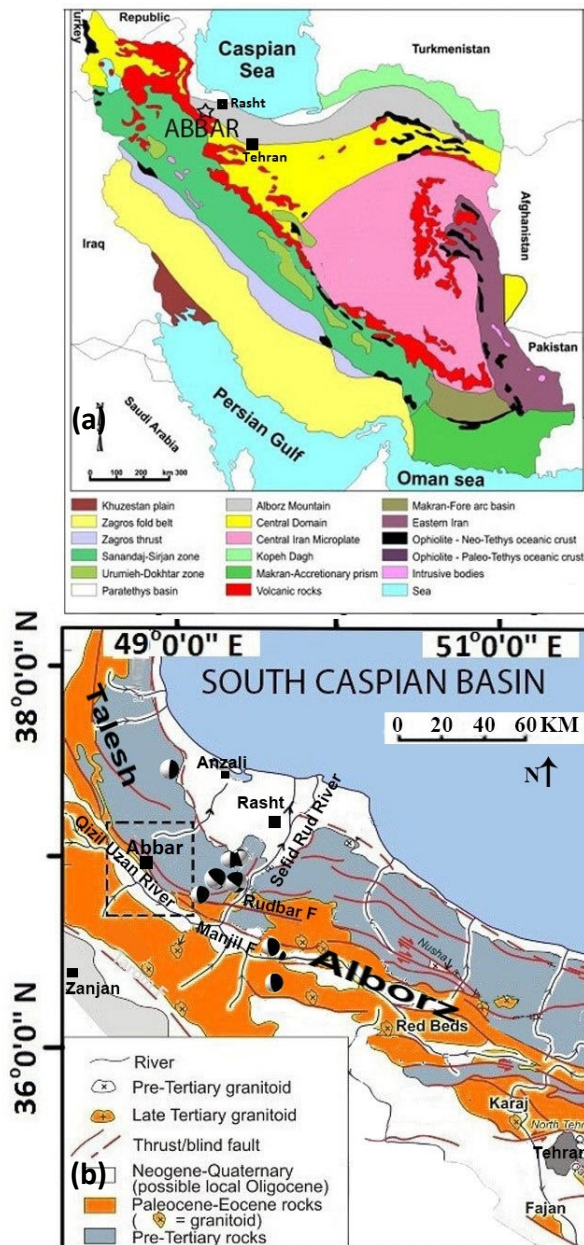


Fig. 1: (a) Location of Abbar area. (b) geological map of Western Alborz and study area. (Adopted from [7]). Fault plane solutions of major earthquakes around study area are shown in fig (b).

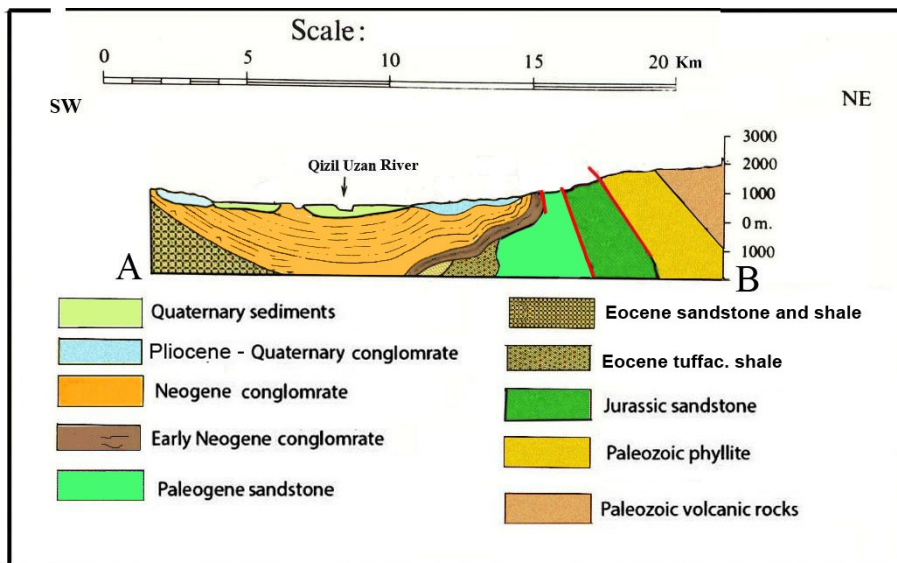


Fig. 2: A profile of study area. This profile is along AB line shown in fig4.

Paleozoic aging rocks include high fractured dark green microdiorite-microgabbro and green phyllite and locally sericite and quartzite. Jurassic rocks include dark gray sandstone with layers of shale (Shemshak Formation). Paleogene rocks are greenish gray sandstone alternated with green tuff or green to yellow crystal tuff and siltstone. Neogene rocks are relatively unconsolidated red conglomerates with gypsiferous marl and gypsum in late Neogene. Pliocene – quaternary rocks are unconsolidated light gray conglomerates.

The study area is located in western Alborz near the Talesh (fig. 1b) but no clear boundary for these structural zones proposed yet. Because of scattered data and great distance between study stations, Geodetic modeling based on GPS and seismic data is not able to solve this problem; so around this area, different deformation models from NE-SW extensional to NW-SE compressional regimes are suggested [27, 28].

This study tries to solve this problem by analyzing area structures and calculating stress directions based on field studies, satellites images and morphotectonic evidences.

Since Abbar Region is located near the epicenter of the Manjil, 1990 catastrophic earthquake and there are abundant historical and instrumental earthquake reports for this region, it is particularly important to study the structural features of this zone to evaluate the earthquake risk.

2- Geological Setting of Study Area

The westward movement of South Caspian Basin (SCB) relative to the approximately NS convergence of the Arabia–Eurasia plates in this region [3] and clockwise rotation of SCB since the mid-Pleistocene period [4], has caused the mutual formation of thrusts and range-parallel (E-W to NW-SE trend) left-lateral strike-slip faults in the Alborz [5,6]. The reverse faults of this area have a dominant direction of N50°W and NE dip direction. The activities of these faults have moved Paleozoic units over younger sedimentary rocks by about 1800 m (Fig.2). Another system of parallel faults with an attitude of N37°E/70°SE is observed in the Abbar region; this system exhibits right-lateral slipping with reverse components. The two mentioned systems have caused rough topographical deformations in the region. This region suffers frequent earthquakes, due to the location of it at the south of SCB [7,8]. The main tectonic characteristics of the area are one of the important controlling factors in morpho-tectonic processes. Deformations of the study area are consistent with the recent activities of the faults [9,10].

The trend of structures in the northwestern Iran matches the suture line of the Iranian-Eurasian plate's collision [11]. During the Precambrian, the Abbar region had been located in the northern margin of Gondwana; however, during the late Triassic, with the closure of the Paleotethys Ocean, it has collided with Eurasia. In the present time, due to the spreading of the Red Sea, this region is subjected to compressional forces [11].

The GPS measurements of motion [12] show that Alborz is shortening by $5 \pm 2 \text{ mm y}^{-1}$, and a left-lateral displacement occurs by $4 \pm 2 \text{ mm y}^{-1}$ rate. After the collision of the Eurasian and Arabian plates, a shortening of $53 \pm 3 \text{ km}$ has occurred in Alborz [13]; near the Abbar area, in the Talesh structural zone, 25–30% shortening occurred after collision by activity of faults [30]. At the present time, the northward motion of Arabian plate toward Eurasia at the rate of $22\text{--}25 \text{ mm y}^{-1}$ [12] have led to the development of deformational structures in the area and fault activity in the Quaternary. The relatively dispersed pattern of faults in the region indicates a deformation rate of several millimeters per year [10, 12, and 14].

Although the active tectonics of Iran is controlled by the northward motion of Arabian plate relative to Eurasia and such direction suggests right-lateral reactivation of northwest-southeast

oriented faults, in this region, faults with this direction are reactivated as left-lateral faults. This might be due to regional changes of stress field which this research tries to describe.

Morphotectonic features can be used to detect deformations created by recent seismic activities [14, 15].

3- Methodology

This research is conducted through three steps; analysis of satellite imagery, field study and observations, and calculating morpho-tectonic indexes. Based on the morpho-tectonic index of the drainage basin asymmetry and structural evidences, a deformation model for the region is proposed. The lineaments extracted from satellite images could be an evidence for subsurface phenomena (e.g. Casas *et al.*2000 [16]). These lineaments were identified by the means of panchromatic images of the IRS satellite **imagery (Pan Sensor)** with a spatial resolution of 6 m and the Landsat ETM⁺ images with a spatial resolution of 30 m. To confirm the fault lineaments and provide information on the active faulting distribution, the extracted lineaments validated through a series of field surveys (e.g. Xypolias and Koukouvelas 2004[17]). The topographic maps of the area were analyzed to calculate the morpho-tectonic indices such as the asymmetry factors and to determine the deformation model of the region.

4- Results

4-1-Remote sensing

Lineaments of the area extracted from satellite images (Fig.3a) using ER Mapper (Ver.7) software and by applying the proper filters such as “SunAngle”, “HighPass”. The Rose Diagrams of these lineaments were sketched based on the length of these lineaments (Fig. 3b).

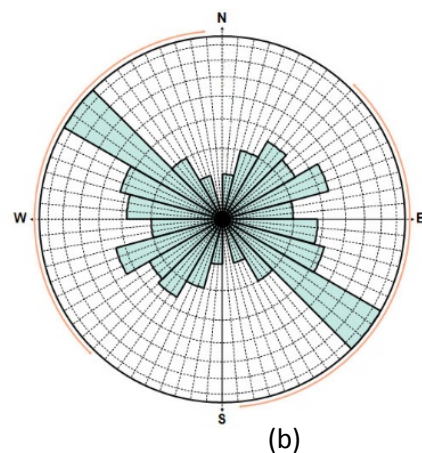
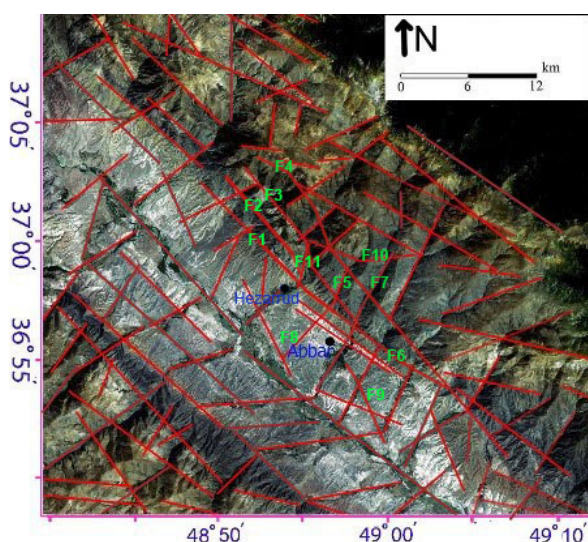


Fig.3: (a) Lineaments map of region extracted from satellite images, (b) Rose Diagram of lineaments based on the length of lineaments.

4-2- Field evidences

The major faults in the area (Fig.4) have delineated by means of two geological maps of Taron and Masouleh sheets [18, 19] and field studies considering satellite images data. *F11* fault was mapped for the first time in this study through satellite images analysis and field surveys. The strike-slip components of *F2*, *F3*, *F4*, *F6*, *F9* and *F10* faults determined by field studies and satellite images data. The slip data of *F9* and *F10* could not be figured by field surveys. They were extracted by satellite images (Fig.5a) and layer displacements (Fig. 5b) which confirms the strike slip component of these faults. *S1* through *S8* are the stations where tectonic structures were surveyed, and kinematic and neotectonic evidences have been measured and recorded as follow:

Station 1 (S1): A U-shaped valley with an approximate length of 150 *m* and N50°E direction was conformed at a relatively unconsolidated Neogene conglomerate. It seems to be a tectonic opening because of tensile stresses perpendicular to the valley direction. Although the rocks of the valley are relatively weathered and unconsolidated, the valley keeps its shape; this indicates a recent formation of the valley (Fig.5c). Within this valley, systematic extensional fissures exist approximately perpendicular to valley direction (Fig.5d).

Station 2 (S2): At this location, in the sandstones (Jurassic), parallel normal faults with an attitude of N50°E/70°SE were recorded (Fig.5e). The rake of net slip confirms the right-lateral slip movement of these faults (Fig.5f).

Station 3 (S3): There are abundant extensional fissures at this location, which have been filled with gypsum fibers (Fig.6 a). The antitaxial fibers are perpendicular to the wall of the fissures and can be an evidence of opening direction [20]. Extensional fissures have approximately S45°E strike (Fig.6 b) and fibers trend is about N40E (Fig.6 c).

Station 4 (S4): At this station, the outcrop of *F4* fault with a reverse left-lateral slip mechanism can be observed (Figs.6d and 6e). Attitude of the fault is S50°E/30°NE and rake of net slip is 35° (Fig.6f).

Station 5 (S5): At this station, the outcrop of the *F11* fault with an attitude of N37°E/75°SE was

recorded (Fig.7a). The rake of net slip is 143° and confirms the reverse right-lateral movement of the fault (Fig.7b).

Station 6 (S6): The extension fissures at this location (Fig.7c) can be used for predicting the type of fault mechanism because they are close to the fault, P-axis inferred from these structures could help determination of fault mechanism (Fig.7d). The attitude of these fissures changes around the end points to about $N71^\circ E/62^\circ NW$ (Fig.7e). The geometry of these fissures and P-axis inferred from them and their position on the south side of the *F3* fault suggests a reverse fault with a left-lateral component.

Station 7 (S7): In this station, the drainage has carved into the Quaternary sediments and formed alluvial fans down streams (fig.8a); this condition is common to almost all of the explored area. According to model of Keller 1986 [21], this condition indicates low rate of uplift relative to the erosion rate in the early Quaternary.

Station 8 (S8): At this station, seven small faults in Neogene conglomerate are visible (Fig.8b). These faults are left-lateral with small normal component (Fig.8c).

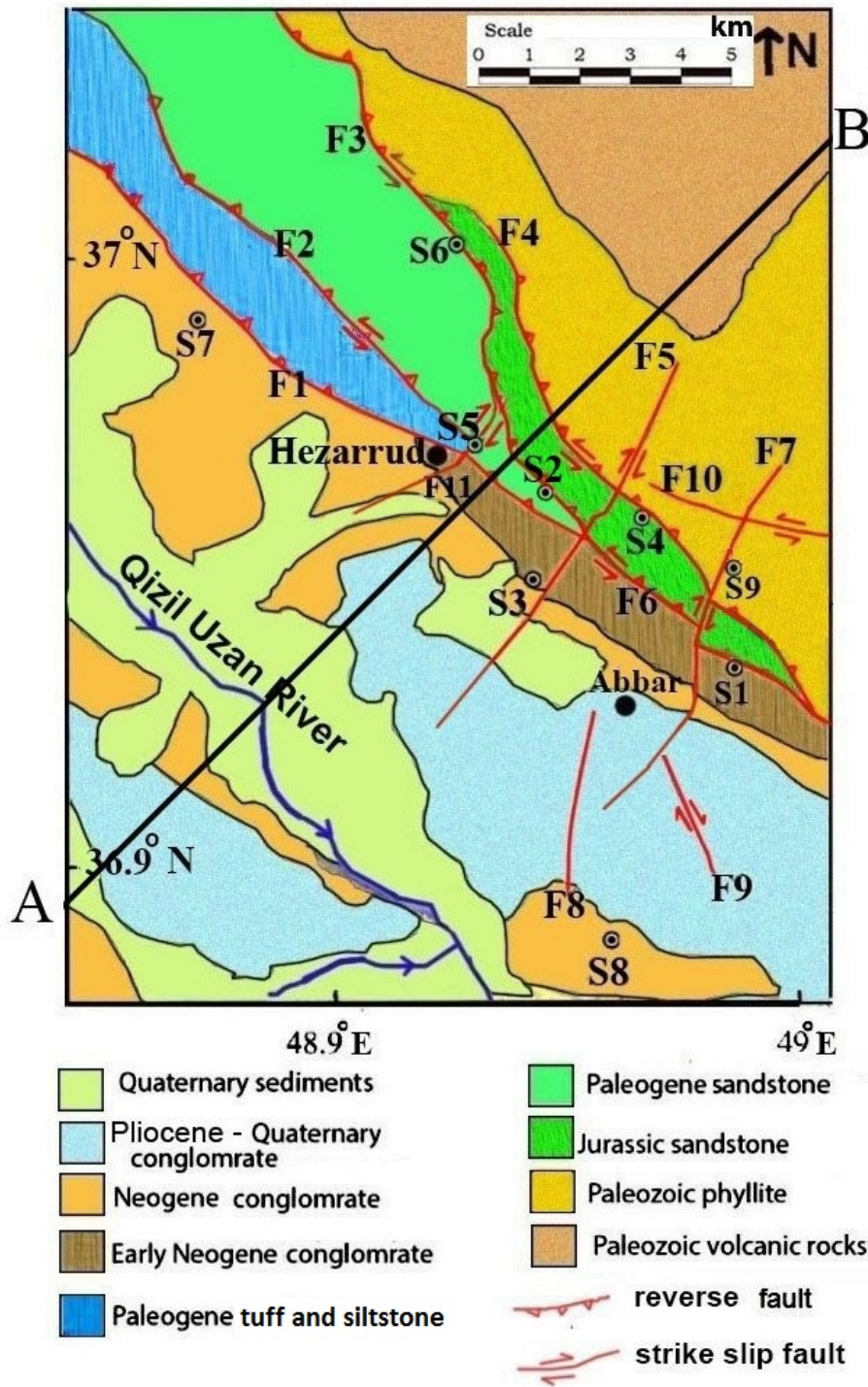


Fig. 4: The modified faults map of the Abbar region. (Base map, Tarom and Masuleh 1:100000 sheets, Geological Survey of Iran [18,19]).

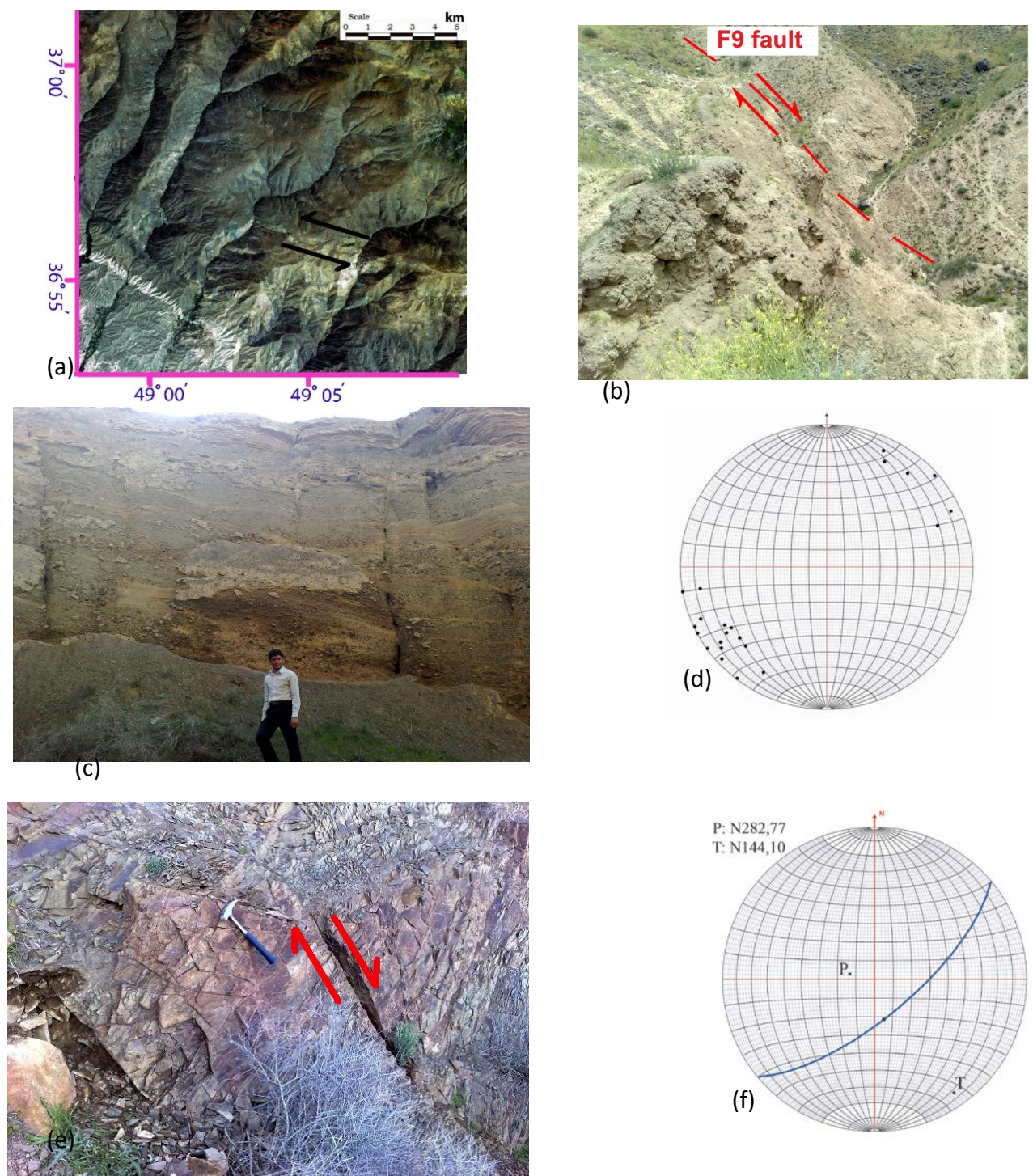


Fig.5: (a) Left lateral displacement of *F10* fault. (b) Right lateral displacement of *F9* fault (view to N). (c) Vertical wall of the valley in *S1* and its extensional fissures (view to Southeast), the steep slope of valley walls indicates a young feature and the effective role of tectonic movement in its formation, (d) Poles of the fissures in *S1* on the Schmidt Net. (e) A normal fault in *S2* (view to SW), and (f) its stereographic projection.

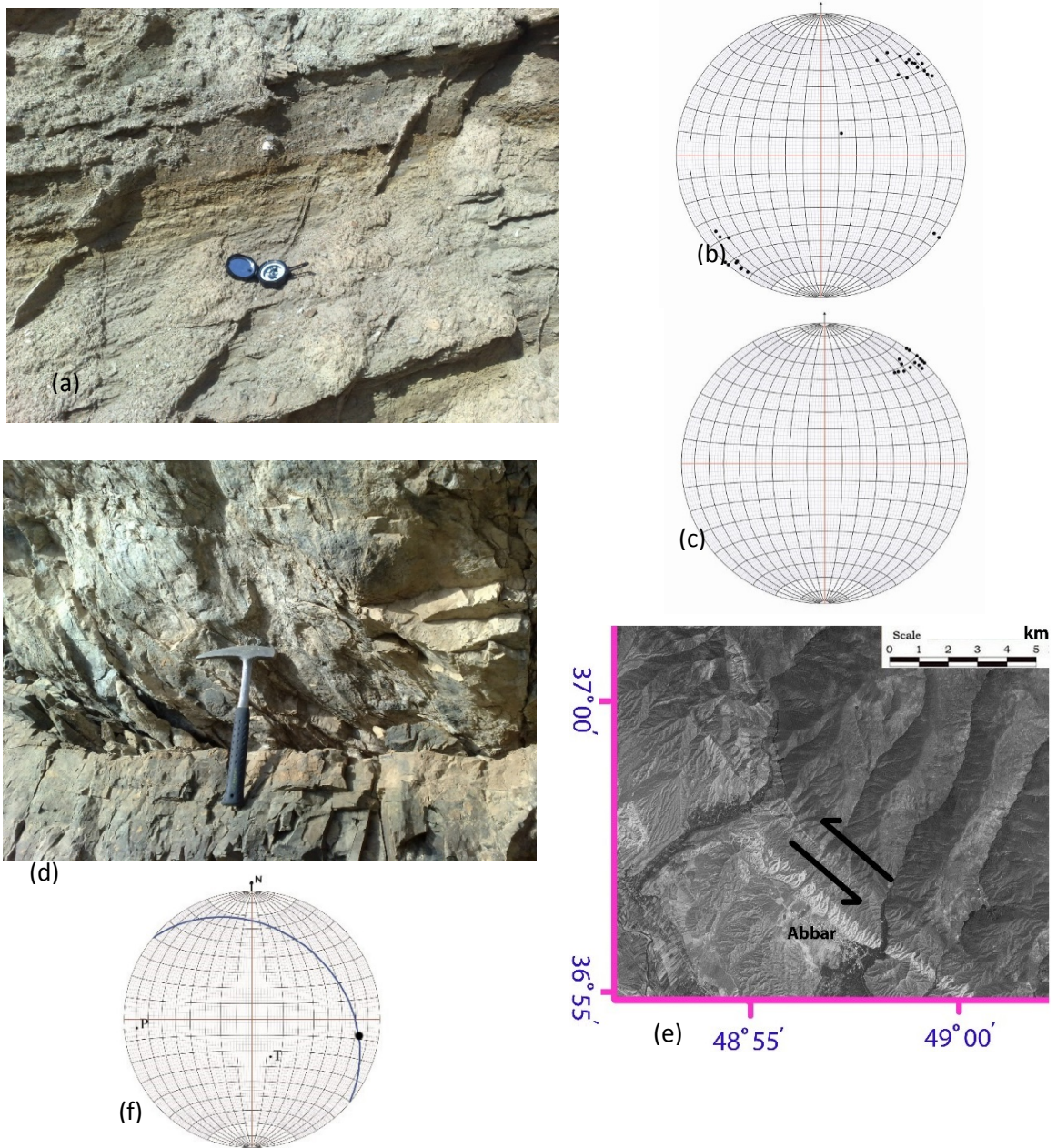


Fig. 6: (a) extension fissures in S3. (b) The poles of fissures in S3. (c) The gypsum fibers direction within the fissures in S3 shows an approximate extension along the N40°E direction. (d) Outcrop of F4 fault, (e) Left lateral displacement of F4 fault. (f) Stereographic projection of F4.

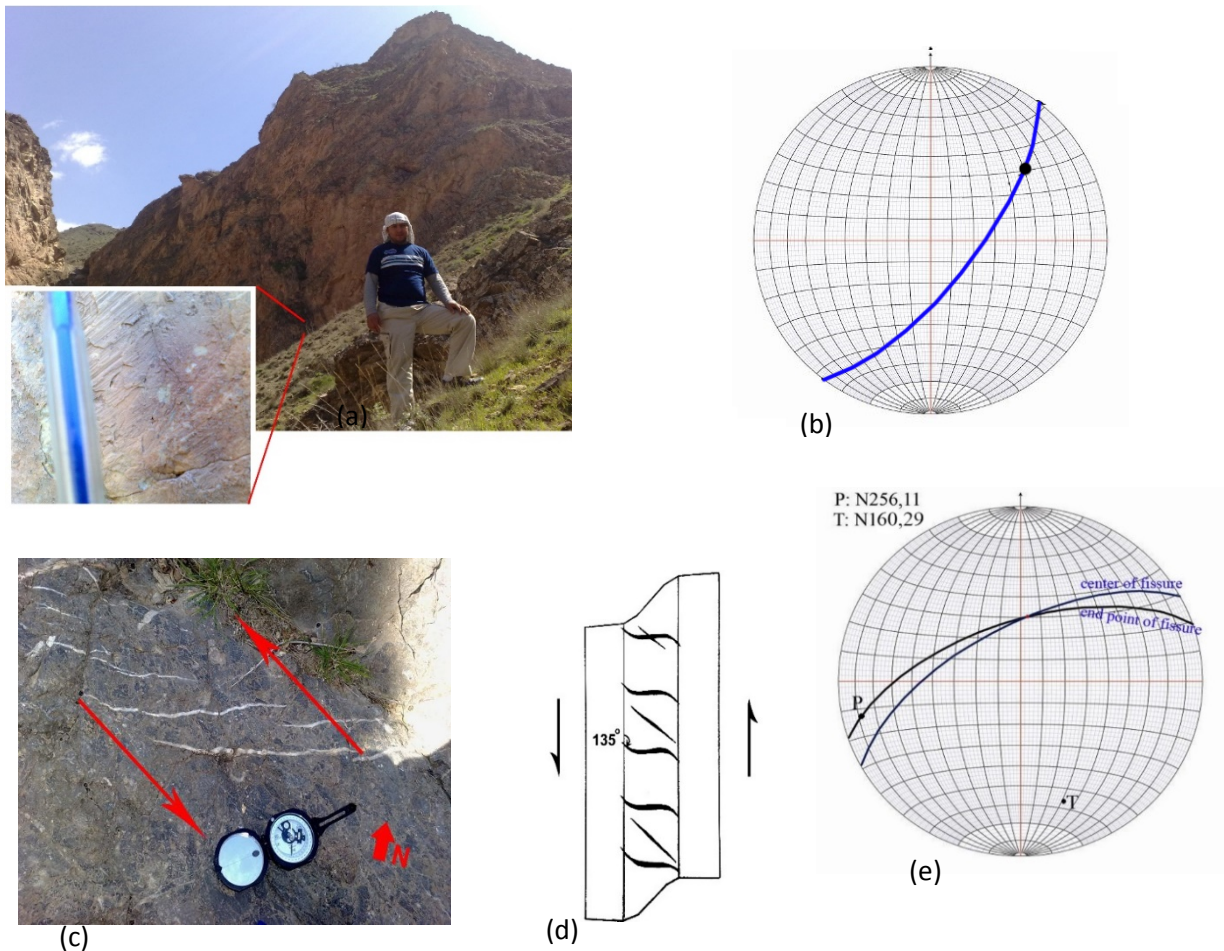


Fig.7: (a) Outcrop of F11 fault (view to NW) and (b) its stereographic projection. Comparing the extension fissures in S6 (c), with the model (d) of Ramsey and Huber 1987 [18]; the attitude of fissures indicates a left-lateral shear. (e) Stereographic projection of the extension fissures and the underlying stresses.

4-3- Analyzing the Qizil Uzan Syncline

In the Abbar Region, the Qizil-Uzan River flows through center of a syncline (Fig.2). Structural analyzing shows that this structure is a cylindrical syncline (Fig.8d) with horizontal axis and σ_1 direction is about N38°E (Fig.8e). The fissures in S₇ and S₃ and gypsum fibers completely match the growth of this syncline and these fissures are parallel to synclinal axis (Figs.8f and 8g)

3-4- Analyzing the fault seismic mechanism

The most significant instrumental earthquake that has occurred near the study area is the Rudbar earthquake of June 20, 1990 (Ms 7.7, Mw 7.3). This earthquake formed three ruptures of Baklor, Kapateh, Zardgoli, and these left-lateral ruptures extend from S85°E to S60°E with

high dip angle with S-SW strike. They have a combined length of approximately 80 km [22].

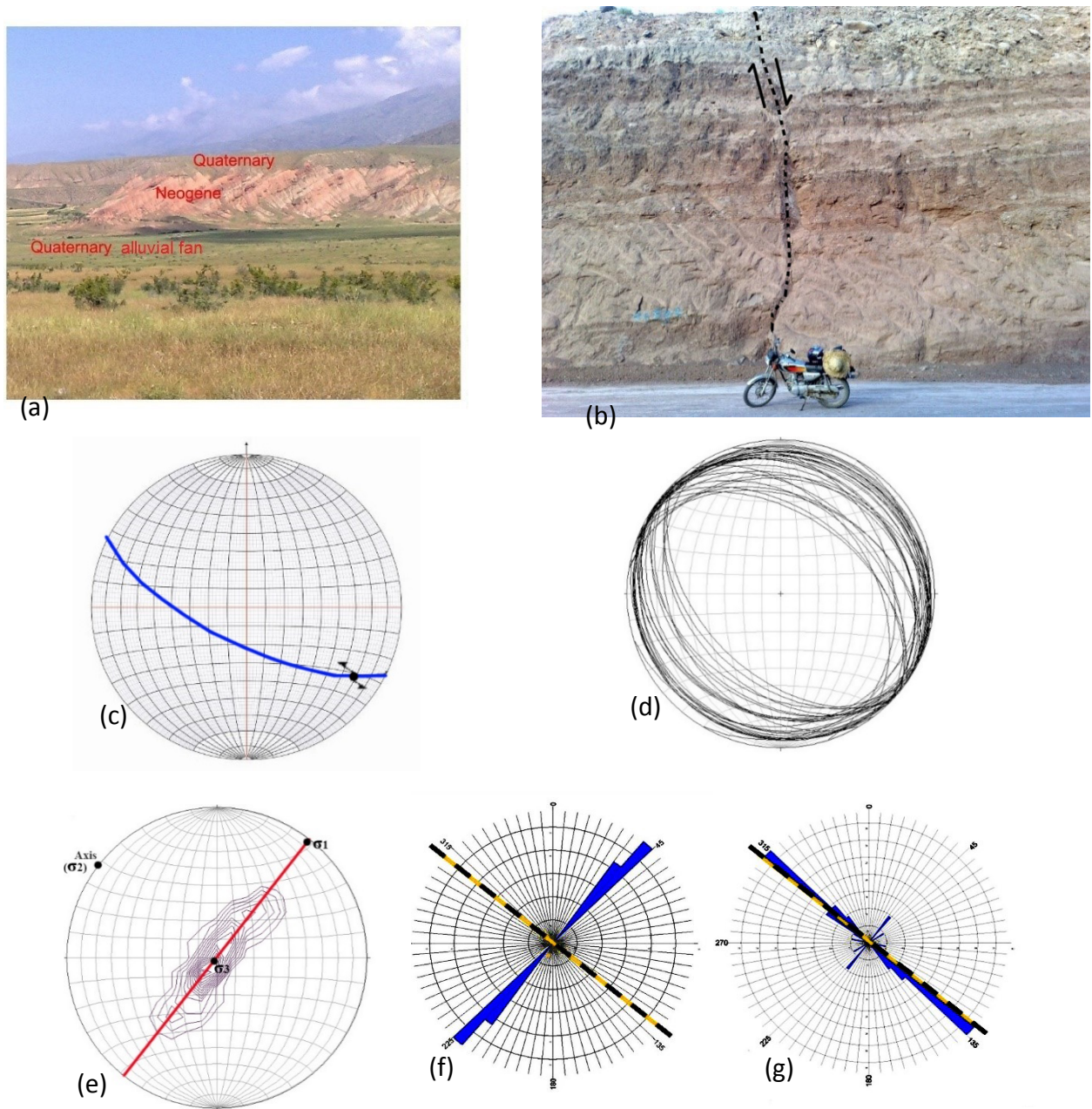


Fig.8: (a) erosion of Quaternary sediments and formation of new alluvial fans in S7 (view to NW). (b) A fault in Neogene conglomerate at station 8 (view to E), and (c) stereographic projection of this fault. (d) Stereographic projection of beddings of Qizil-Uzan Syncline. (e) Structural Analysis of the Qizil-Uzan syncline. (f) Rose Diagram of gypsum fibers within the veins of S3, and (g) fissures of S3; axial surface of the Qizil-Uzan syncline denoted with dashed line.

Since the epicenter of this earthquake (with a left-lateral mechanism) is very close to that of the 1983 earthquake (Mb 5.6, Ms 5.0) with a reverse mechanism, it appears that the oblique

shortening of Alborz is differentiated into reverse and left-lateral strike-slip [22].

Eight years after the major earthquake event in Rudbar (1998), micro-seismic information of the region recorded and analyzed the by means of a dense local network and calculated the *P*-axis direction [23]. The obtained results show WSW-ENE direction for maximum stress and confirm that the direction of maximum stress in this area, at least locally, is different from stress direction expected from NS convergence of the Arabia–Eurasia plates.

The stress directions obtained from fault plane solution (Fig.1b) (present-time stresses), used for calculating stress direction by the method of Delvaux and Sperner 2003[24] (Fig.9).

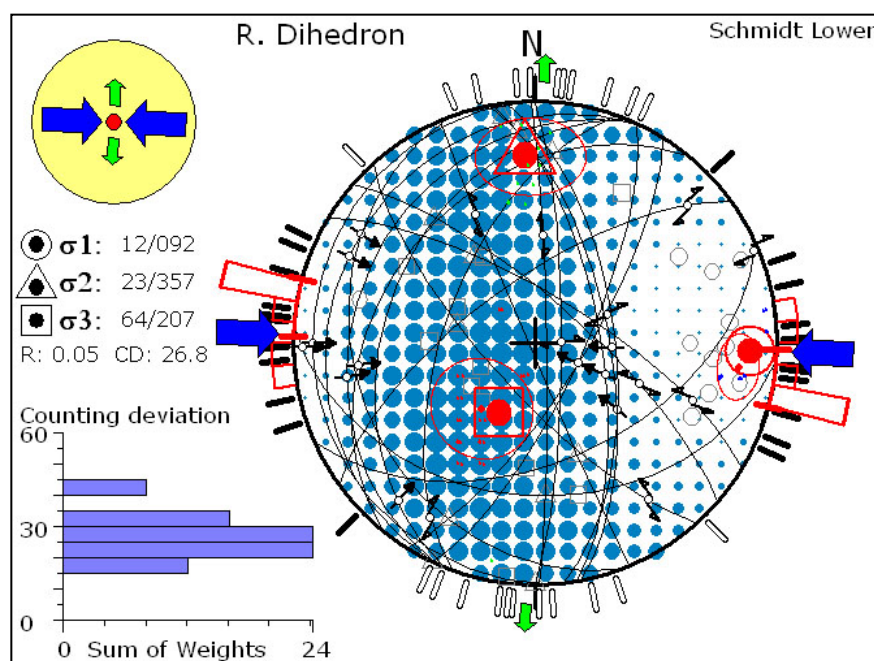


Fig.9: Stresses direction based on the instrumental earthquakes data around Abbar town.

4-5- Geomorphological index of asymmetry factor

The geomorphological index of asymmetry factor was computed and analyzed for valleys in this area (for more details refer to [25]). Five valleys (V1-V5) have been analyzed by using the asymmetry index of the drainage basin (Fig.10). The arrows show the tilting direction at each location and the numbers indicate the index values. The tilting directions of V3 and V4 are opposite to each other, which may indicate a syncline-like tilting. The changes of arrow directions at the south of valleys V1 through V3 (denoted with F in Fig.10) closely agree with F3 and F6 faults. The syncline-like tilting shows that an approximately E-W stress direction might

act on the study area.

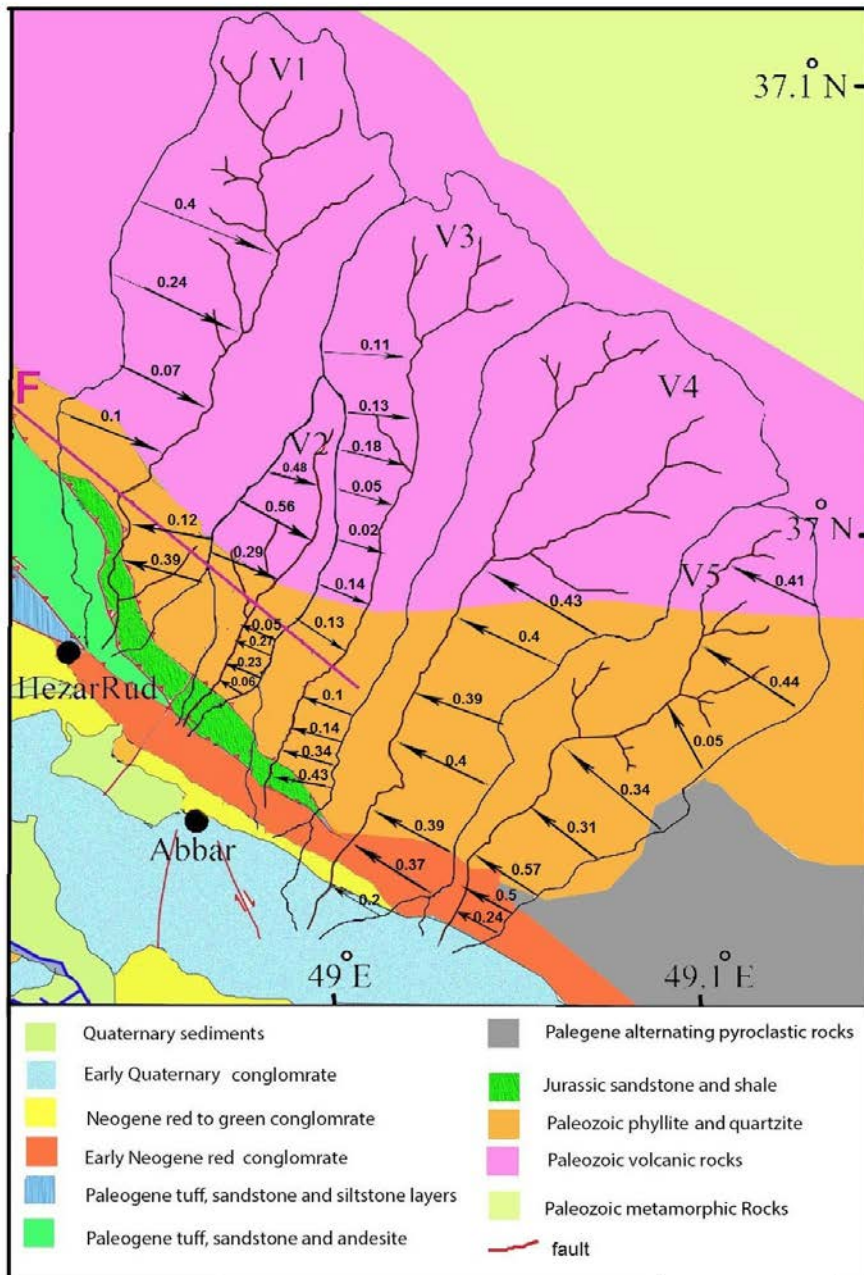


Fig. 10: Analysis of 5 valleys (V1-V5) using the asymmetry factor index of the drainage basin. The arrows show the tilting direction at each location and the numbers indicate the index values. The directions of V4 and V5 are opposite to each other, which may indicate a syncline-form tilting. The changes of arrow directions at the south of valleys V1 through V3 (denoted with F on the map) approximately agree with Faults F3 and F6.

5- Discussion

Study area is between Alborz and Talesh structural zones and no clear boundary for these

structural zones proposed yet. Previous works about stress condition in this part of Iran are general and they resulted different conclusions about Alborz and Talesh zones. This paper tries to specify local stress condition in the area.

The stress directions resulted from fault plane solution, differ from stresses responsible for Qizil-Uzan syncline forming. It is appear that each fault activity may have different focal mechanism and this method may not offer the exact direction of stresses governing the region. Thus, faults slip and other data obtained from stations were used to calculate stress directions applying the Win Tensor software introduced by Delvaux and Sperner 2003[24]. The results (Fig.11) show that σ_1 direction is very close to E-W. This direction might not be responsible for Qizil-Uzan syncline forming. Such discrepancy could be interpreted as a regionally change in stress direction after forming the syncline. The evidence of tilting valleys and seismic data confirm such change. The change in stress may affect the deformation model of the region. The pattern of faults movement in the region and results of the lineaments rose diagrams extracted from satellite images resembles the left-lateral shear model (Fig.12) according to McClay1987 [26]. However, an obvious difference that can be observed between the model and area structural condition is that the P fractures have extended more than the R_1 fractures; this assumption leads to classify main faults such as $F4$ and $F6$ as P fractures which is an unusual condition. The reason for their abundance relative to the R_1 faults is that they have existed prior to the formation of the shear stress zone. The P fractures are approximately parallel to Qizil-Uzan syncline's axis and perpendicular to maximum stress direction that formed this syncline; thus, they were reverse faults when syncline formed. The slip vector rake in the $F4$ fault is about 35° , which shows that the horizontal displacement surpasses the vertical displacement; however the vertical displacement is too great to be explained by a shear model. Probably, left-lateral shear is rather recent and before that, these faults acted as reverse faults.

Regarding the conditions in $S7$ that is common to almost all of the explored area, the drainages of the region have eroded the Quaternary sediments and deposited them as alluvial fans downstream. This shows that in the Quaternary period, the rate of folding and uplift of the layers has become very slow and the erosion rate has overtaken the rate of uplift; otherwise, the more recent Quaternary sediments should have been above the older sediments. Transformation of reverse activity of faults to a left-lateral shear regime at the recent

Quaternary may cause the slow uplift rate.

As is observed in the left-lateral shear zone model, there are tension structures (normal faults) and tension fractures perpendicular to σ_3 . The valley observed at Station-1, the normal faults observed at Station-2 and the extension fissures at Station-6 might be assumed as this tension structures. However, their forming maximum stress direction is between stresses responsible for syncline and shear model. They might be an evidence for gradually change of stress.

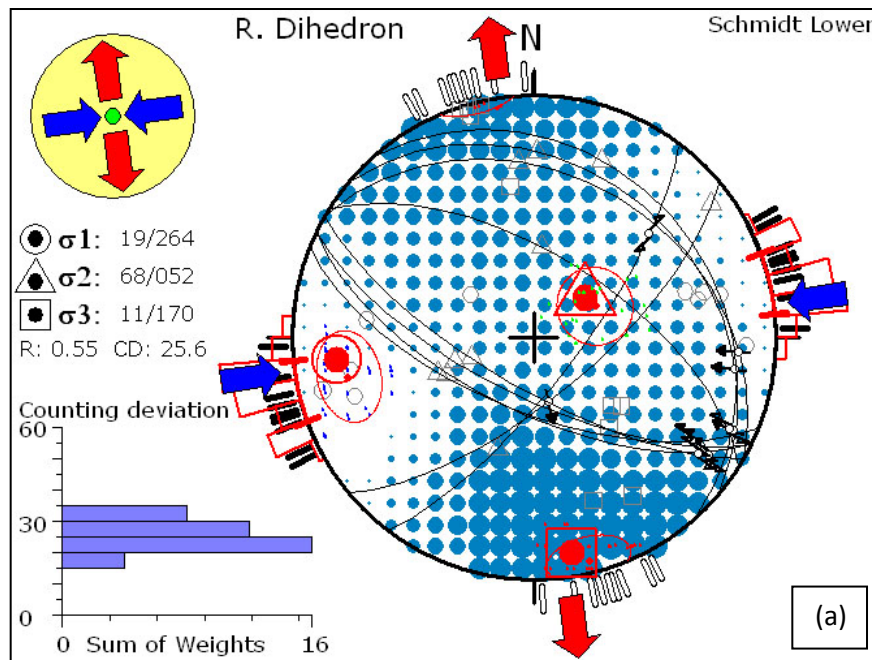


Fig. 11: A summary of the stresses based on the fault slip data in stations.

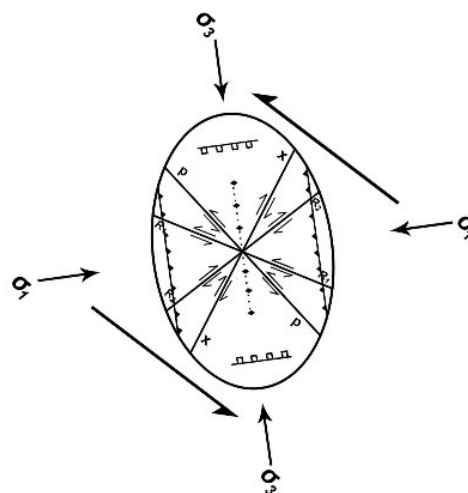


Fig. 12: left-lateral shear model of McClay 1987 [24] rotated to match area stresses direction

calculated from the fault slip data.

6- Conclusions

The stress directions and the rheology of rocks and structures in the Abbar region show that a variety of deformations has occurred in the area. The geomorphological evidences such as fault scarps, Quaternary displacements and stream shifts indicate a high tectonic activity in the region. The major faults of the north of Abbar area can be divided into two groups with approximate directions of S50°E and N37°E. The first group consists of the faults that based on the existing folds and morpho-tectonic evidence, have had reverse mechanism before the Quaternary, however, now display a left-lateral mechanism with a reverse component. Evidences such as fault scarps and extension fractures suggest that these two groups of faults constitute *P* and *R*₂ type fractures in a shear zone, respectively, where shear occurs along an approximate S60°E direction. The reason for more extensive *P* fractures relative to *R*₂ fractures is that the *P* fractures have already existed in the form of reverse faults (however, following the changes of stress directions) have become active as strike-slip faults. The directions of the Qizil-Uzan syncline and older faults indicate that pre-Quaternary maximum stress direction was about N39°E; however, this direction has now changed locally to S84°W. This change of stress direction has altered the mechanism of older faults and formed a shear zone.

References

1. Wesnousky SG, Bormann JM, Kreemer C, Hammond WC, Brune JN. Neotectonics, geodesy, and seismic hazard in the Northern Walker Lane of Western North America: Thirty kilometers of crustal shear and no strike-slip? *Earth and Planetary Science Letters*. 2012; 329-330: 133–140.
2. Cloetingh S, Cornu T, Ziegler PA, Van Eck T. Neotectonics and interpolate continental topography of the northern Alpine Foreland. *Earth-Science Reviews*. 2006; 74(3): 127-196.
3. Copley A, Jackson J (2006) Active tectonics of the Turkish-Iranian Plateau. *Tectonics*, 25, TC6006.
4. Ritz JF, Nazari H, Ghassemi A, Salamati R, Shafei R, Solaymani S, Vernant P. Active transtension inside central Alborz: A new insight into northern Iran–southern Caspian geodynamics. *Geology*. 2006; 34, 477–480.
5. Allen MB, Ghassemi MR, Shahrabi M, Qorashi M. Accommodation of late Cenozoic oblique shortening in the Alborz range, northern Iran. *Journal of Structural Geology*. 2003,a; 25, 659–672.

6. Allen MB, Vincent SJ, Alsop GI, Ismail-zadeh A, Flecker R. Late Cenozoic deformation in the South Caspian region: effects of a rigid basement block within a collision zone. *Tectonophysics* 366, 2003,b; 223– 239.
7. Rezaeian M. Coupled tectonics, erosion and climate in the Alborz Mountains, Iran. PhD thesis, University of Cambridge. 2008
8. Berberian M, Yeats RS . Contribution of archeological data to studies of earthquake history in the Iranian Plateau. *Journal of Structural Geology*. 2001; 23, 563–584.
9. Walker R, Jackson J. Active Tectonics and Late Cenozoic Strain Distribution in Central and Eastern Iran. *Tectonics*, 2004; 23, 5,157-170
10. Meyer B, Le Dortz K. Strike-Slip Kinematics in Central and Eastern Iran: Estimating Fault Slip-Rates Averaged over the Holocene: *Tectonics*, 2007; 26, TC5009, p20.
11. Berberian M, King GCP. Towards a paleogeography and tectonic evolution of Iran. *Canadian Journal of Earth Science*, 1981; 18, 210-256.
12. Vernant Ph, Nilfroushan F, Hatzfeld D, Abbassi MR, Vigny C, Masson F, Nanakali H, Martinod J, Ashtiani A, Bayer R, Tawakoni F, Chery J. Contemporary Crustal Deformation and Plate Kinematics in Middle East Constrained by GPS Measurements in Iran and Northern Oman. *Geophysical Journal International*, 2004; 157, 381–398.
13. Guest B, Axen GJ, Lam PS, Hassanzadeh J. Late Cenozoic shortening in the west-central Alborz Mountains, northern Iran, by combined conjugate strike-slip and thin-skinned deformation. *Geosphere*, 2006; 2, 35-52.
14. Walker RT, Gans P, Allen MB, Jackson J, Khatib M, Marsh N, Zarrinkoub M. Late Cenozoic Volcanism and Rates of Active Faulting in Eastern Iran: *Geophysical Journal International*, 2009; 177, 783–805.
15. McBride JH, Nelson ST, Heiner BD, Tingey DG, Morris TH, Rey KA. Neotectonics of the Sevier Desert basin, Utah as seen through the lens of multi-scale geophysical investigations. *Tectonophysics*. 2015; 654: 131–155.
16. Casas AM, Corte S, Angel L, Maestro A, Soriano MA, Riaguas A, Bernal J. A program for lineament length and density analysis. *Computers and Geosciences*, 2000; 26, 1011-1022.
17. Xypolias P, Koukouvelas IK. Fault Trace Parameters as a Tool for Analyzing Remotely Sensed Fault Rays: An Example from the Eastern Gulf of Corinth, Greece. *Journal of Remote Sensing*, 2004; 25, 4685-4699.
18. Ministry of Economy, Geological Survey of Iran , *Geology of the Tarom district, western part (Zanjan area, northwest Iran)*, 1966.
19. Ministry of Economy, Geological Survey of Iran , *Geology of the Masuleh sheet, 1:100,000, northwest Iran*, 1972.
20. Ramsay JG, Huber MI. *The techniques of modern structural geology*. Academic Press London .1987; vol. 1.
21. Keller EA. *Investigation of active tectonics: use of surficial earth processes*. Active tectonics, National Academy press. 1986.

22. Berberian M, Qureshi M, Jackson JA, Priestly K, Wallace T. The Rudbar-Tarom earthquake of 20 June 1990 in NW Persia: Preliminary field and seismological observations, and its tectonic significance. *Bulletin of the Seismological Society of America*, 1992; 82, 1726-1755.
23. Tatar M, Hatzfeld D. Microseismic evidence of slip partitioning for the Rudbar-Tarom earthquake (Ms 7.7) of 1990 June 20 in NW Iran, *Geophys. J. Int.* 2009; 176, 529–541.
24. Delvaux D, Sperner B. Stress tensor inversion from fault kinematic indicators and focal mechanism data: the TENSOR program. In: *New Insights into Structural Interpretation and Modelling* (D. Nieuw land Ed.). Geological Society, London, Special Publications, 2003; 212: 75-100.
25. Keller EA, Pinter N. *Active Tectonics: Earthquakes and Landscape*. Second Edition. Prentice-Hall: Upper Saddle River. 2002
26. McClay K. *The mapping of geological structures*. Geological Society of London Hand book press. 1987.
27. Masson, F., Lehujeur, M., Ziegler, Y. and Doubre, C., (2014), Strain rate tensor in Iran from a new GPS velocity field. *Geophysical Journal International*, 509.
28. Zarifi, Z., Nilforoushan, F. and Raeesi, M. (2014), Crustal Stress Map of Iran: Insight from Seismic and Geodetic Computations. *Pure and Applied Geophysics* 171: 1219-1236.
29. Djamour, Y., Vernant, P., Bayer, R., Nankali, H., Ritz, J., Hinderer, J., Hatam, Y., Luck, B., Moigne, N., Sedighi, M., and Khorrani F. (2010), GPS and gravity constraints on continental deformation in the Alborz mountain range, Iran. *Geophys. J. Int.* 183, 1287–1301.
30. Madanipour. S., A. Yassaghi, T.A. Ehlers, E. Enkelmann, (2018), Tectonostratigraphy, structural geometry and kinematics of the Talesh Mountains, Insights to the Late Cenozoic deformation pattern at NW Iranian Plateau margin, *American Journal of Sciences*, Vol. 318, No.2.

Figures Captions:

Fig. 1: (a) Location of Abbar area (b) geological map of Western Alborz and study area. (Adopted from [7]. Fault plane solution of great earthquakes around study area are shown in fig(b);

Fig. 2: A profile of study area. This profile is along AB line shown in fig4.

Fig.3: (a) Lineaments map of region extracted from satellite images, (b) Rose Diagram of lineaments based on length of lineaments.

Fig. 4: The modified faults map of the Abbar region. (Base map, Tarom and Masuleh 1:100000 sheets, Geological Survey of Iran [18,19]).

Fig.5: (a) Left lateral displacement of *F10* fault. (b) Right lateral displacement of *F9* fault (view to N). (c) Vertical wall of the valley in *S1* and its extensional fissures (view to Southeast), the steep slope of valley walls indicates a young feature and the effective role of tectonic movement in its formation, (d) Poles of the fissures in *S1* on the Schmidt Net. (e) A normal fault in *S2* (view to SW), and (f) its stereographic projection.

Fig. 6: (a) extension fissures in *S3*. (b) The poles of fissures in *S3*. (c) The gypsum fibers direction within the fissures in *S3* shows an approximate extension along the $N40^{\circ}E$ direction. (d) Outcrop of *F4* fault, (e) Left lateral displacement of *F4* fault. (f) Stereographic projection of *F4*.

Fig.7: (a) Outcrop of *F11* fault (view to NW) and (b) its stereographic projection. Comparing the extension fissures in *S6* (c), with the model (d) of Ramsey and Huber (1987); the attitude of fissures indicates a left-lateral shear. (e) Stereographic projection of the extension fissures and the underlying stresses.

Fig.8: (a) erosion of Quaternary sediments and formation of new alluvial fans in *S7* (view to NW). (b) A fault in Neogene conglomerate at station 8 (view to E), and (c) stereographic projection of this fault. (d) Stereographic projection of beddings of Qizil-Uzan Syncline. (e) Structural Analysis of the Qizil-Uzan syncline. (f) Rose Diagram of gypsum fibers within the veins of *S3*, and (g) fissures of *S3*; axial surface of the Qizil-Uzan syncline denoted with dashed line.

Fig.9: Stresses direction based on the instrumental earthquakes data around Abbar town.

Fig. 10: Analysis of 5 valleys (*V1-V5*) using the asymmetry factor index of the drainage basin. The arrows show the tilting direction at each location and the numbers indicate the index values. The directions of *V4* and *V5* are opposite to each other, which may indicate a syncline-form tilting. The changes of arrow directions at the south of valleys *V1* through *V3* (denoted with *F* on the map) approximately agree with Faults *F3* and *F6*.

Fig. 11: A summary of the stresses based on the fault slip data in stations. These diagrams are made by Win tensor software that is provided by [24].

Fig. 12: left-lateral shear model of McClay 1987, [24] rotated to match area stresses direction calculated from the fault slip data.